Tech Science Press

Corrosion Performance of Stainless Steel Reinforcement in the Concrete Prepared with Seawater and Coral Waste and Its Ecological Effects

Xingguo Feng[1,2,3], Yiji Zhang[1], Xiangyu Lu[1,*], Yiwen Xu[1], Leyuan Zhang[1], Chao Zhu[1], Tong Wu[1], Yashi Yang[4] and Xuhui Zhao[5]

[1]Jiangsu Key Laboratory of Coast Ocean Resources Development and Environment Security, Hohai University, Nanjing, 210098, China
[2]State Key Laboratory of Green Building Materials, Beijing, 100024, China
[3]Key Laboratory of Marine Materials and Related Technologies, Ningbo Institute of Materials Technology and Engineering, Chinese Academy of Sciences, Ningbo, 315201, China
[4]College of Water Conservancy Engineering, Wanjiang University of Technology, Maanshan, 243000, China
[5]School of Materials Science and Engineering, Beijing University of Chemical Technology, Beijing, 100029, China
*Corresponding Author: Xiangyu Lu. Email: luxiangyu@hhu.edu.cn
Received: 30 December 2019; Accepted: 23 March 2020

Abstract: Durability and ecological effects of the stainless steel reinforced coral waste concrete were compared with those of the carbon steel reinforced ordinary concrete. The results showed that the corrosion current densities of the stainless steel in the coral waste concrete were less than one-tenth of those of the carbon steel in the same grade ordinary concrete. The stainless steel in the seawater coral waste concrete maintained passivation even after more than two years of immersion in 3.5% NaCl solution, while the carbon steel counterparts in the ordinary concrete were seriously corroded under the same condition. Simultaneously, the corrosion current density of the stainless steel reinforcement decreased slightly with the strength grade of the coral waste concrete. The ecological evaluation indicated that the non-renewable energy consumption and CO_2 emission of per cubic meter of the newly constructed stainless steel reinforced coral waste concrete were 23.72% and 1.419% less than those of the carbon steel reinforced ordinary concrete with the same grade, while the aforementioned two parameters of the former material were reduced by 44.81% and 32.0% in comparison to the latter one in 50 years duration.

Keywords: Coral waste; stainless steel; seawater; green concrete; corrosion

Nomenclature

NREC	non-renewable energy consumption
CE	CO_2 emission
CWC	coral waste concrete
CS	Q235 carbon steel
304SS	304 stainless steel
2205SS	2205 duplex stainless steel
OC	ordinary concrete

OCP	open circuit potential
LPR	linear polarization resistance
i_{corr}	corrosion current densities
SCE	saturated calomel electrode
EIS	electrochemical impedance spectroscopy
R_p	polarization resistance (LPR)
HSS2	low-Ni austenoferritic stainless steel
HPC	high-performance concrete
R_s	solution resistance
R_{con}	concrete resistance
R_{ct}	polarization resistance (EIS)
CPE_{con}	concrete capacitance
CPE_{ct}	double layer capacitance
CPE	constant phase element

1 Introduction

Many structures need to be constructed on the tropical islands far from the mainland in the ocean exploitation [1]. Steel-reinforced concrete, which generally exhibits satisfying durability, is the ideal structural material in the corrosive tropical marine environment. However, the transportation of the raw materials, like the crushed stone aggregate and river sand from the mainland, will consume tremendous energy as well as emit massive CO_2. As the Green Building Challenge Handbuch [2] reported, the non-renewable energy consumption (NREC) and CO_2 emission (CE) of shipping are 0.13 MJ Km^{-1} T^{-1} and 0.0089 kg Km^{-1} T^{-1}, respectively. Thus, utilizing the coral waste on the islands to replace the ordinary raw materials is a cleaner way to produce concrete.

On the coral reef abundance tropical island, massive coral waste was generated in the waterway dredging, wharves construction, oil well construction, as well as some other marine engineering projects [1]. Many scientists attempted to apply the coral waste to produce concrete in recent years [3–7]. Compared with the conventional crushed stone aggregate, the coral waste aggregate exhibits high porosity, low specific gravity, and strong water absorption [4], which causes that the coral waste concrete (CWC) obviously differs from the ordinary concrete (OC). Firstly, many attentions were attracted on the improvement of the mechanical properties of the CWC. Arumugam et al. [3] systematically investigated the mechanical properties of the coral aggregate and noticed that its crushing, impact, as well as abrasion values were higher than those of the conventional crushed stone aggregate. Moreover, the concrete prepared with the coral aggregate needs more water than the ordinary concrete counterpart produced with the conventional crushed stone aggregate, and the strengths of the former concrete samples were lower than those of the latter ones. In fact, the strength of the coral concrete can reach ~30 MPa easily, but the higher strength coral concrete will be limited by the strength of the coral aggregate. Therefore, the coral concrete was suggested to be applied in the low-rise buildings on the islands or reefs [3]. In another study, Wang et al. [5] compared the compressive strength of the concrete prepared by applying the coral sand together with ordinary gravel to that of the concrete mixed with river sand and ordinary gravel, and they noticed that the compressive strength of the one containing the coral sand was always higher than that of the sample prepared by using the river sand. This situation was ascribed to the dense interfacial transition zone, as well as the interlocking between the coral sand and cement paste matrix, which caused by that the hydration products filled into the pore space of the coral sand. Recently, Cheng and co-authors [6] also studied the strength of the coral sand concrete, in which the cementitious materials were replaced by different

content of fly ash, slag, and metakaolin, respectively. The results showed that the early strength of the coral sand concrete was slightly higher than that of the river sand concrete while the final strength (28 d) of the former concrete became lower than that of the latter one. Moreover, fly ash and metakaolin corresponding significantly diminished and enhanced the strength of the coral sand concrete. Simultaneously, the metakaolin could reduce the drying shrinkage and the chloride diffusion coefficient of the coral sand concrete. Hence, it was proposed to be a supplementary cementitious material, togethers with the coral sand to be used in CWC on the open islands. However, Wu et al. [7] studied the influence of fly ash and silica fume on the strength of the concrete prepared with coral aggregate and coral sand, and noticed that fly ash reduced the early-age strength and enhanced the later-age strength while silica fume always enhanced the strength of the CWC. In general, some contradictory conclusions were reported in literatures [3–7], and more investigation should be performed to understand the mechanical properties of the CWC.

The corrosive of the tropical marine climate, as well as the aggressive anions contained in the coral waste aggregates can accelerate the corrosion of the steel reinforcement in concrete. Thus, some scientists [4,8] thought that the steel reinforcement was unsuitable to be applied in the CWC, and the non-metallic fibers were potential candidates for reinforcing the coral concrete in the structures on the tropical marine islands or reefs. However, Wang and co-authors [9,10] studied the mechanical properties of the CWC contained various contents of carbon fiber, polypropylene fiber, as well as sisal fiber, and reported that the strengths of the CWC initially increased with the contents of the fibers and then decreased with the further increasing contents. Simultaneously, the fibers enhanced the flexural strength significantly, whereas increased the compressive strength of the CWC slightly [9]. Unfortunately, the fibers were difficult to be uniformly distributed in the CWC [11–13], similar to those in the OC, which may cause the unstable mechanical properties of the CWC and reduce the safety of the structures. Therefore, more attentions should be paid on the dispersion issue of the fiber CWC.

There can be little doubt that the corrosion of steel reinforcement was accelerated by the aggressive anions (Cl⁻) in the CWC, but the effect of Cl⁻ in the raw materials was not the critical factor. Ehlert [14] reported that the Timing Bunker, a building constructed by applying the steel-reinforced CWC at Bikini Atoll, was still in excellent condition after 20 years of service. Furthermore, after investigating the quality of three coral concrete structures and their surrounding environments, the author [14] concluded that the surrounding environment, the concrete cover thickness, and the crack width of concrete were the determining factors to the corrosion of the CWC structure, while the corrosive anions in the coral waste and seawater were not the primary causes of the rapid structural deterioration. Another study performed by Kakooei et al. [4] indicated that the corrosion rate of carbon steel rebar in the CWC doubled when compared with the counterpart in the OC with the same grade. On the other hand, many studies [15–17] showed that the chloride thresholds of various types of stainless steel (SS) are 10 to 100 times higher than that of the carbon steel (CS), while the corrosion rate of the former steel is only 1/10 or even 1/1000 of that of the latter steel in the OC [18]. Consequently, it is easy to deduce that the corrosion rate of stainless steel in the CWC would be obvious lower than that of the carbon steel in the OC, after comprehensively considering the results reported in previous studies [15–18]. Thus, the application of SS reinforcement in the CWC may be one of the candidate methods to solve the durability issue of the structures on the tropical marine islands and reef.

Based on the aforementioned reviews of the literature, the utilization of the CWC in the structures was limited by the low strength and its aggressivity on the tropical islands far from the mainland. The SS rebar was applied to reinforce the CWC for producing high bearing capacity and durable concrete structures, which also could be one cleaner way to build marine structures on those tropical islands. The corrosion performances of 304 and 2205 stainless steel reinforcement in different grades CWC was compared with those of the carbon steel in the C30 OC, via the open circuit potential (OCP), linear polarization

resistance (LPR), electrochemical impedance spectroscopy (EIS), as well as polarization curves measurements, respectively. Furthermore, the corrosion state of the stainless steel reinforcement in CWC and the carbon steel in the OC was examined after 750 days of immersion. In the present study, the corrosion behavior of SS reinforcement in low strength ($\leq$ C30) CWC were investigated, and those of SS samples in the high-strength CWC should be studied in the further study. The results could provide reference values for the design of stainless steel reinforced coral concrete structure, as well as support the estimation the life-time of the coral concrete structure in the tropical marine environment.

2 Materials and Methods

2.1 Materials

Three types of commercial plain round steel rebar (Φ10 mm), including Q235 carbon steel (CS), 304 stainless steel (304SS), as well as 2205 duplex stainless steel (2205SS) was used. According to previous studies [19–22], the solution containing 0.1 mol/L NaOH, with a pH value of 13, was adopted to simulate the concrete pore solution. The rebar sample, with 60 mm length, was abraded to No. 600 emery papers. The steel samples were degreased and washed by using ethanol and deionized water in turn, then a copper wire was soldered on the end of rebar. Thereafter, both ends of the steel sample were coated with silica gel, leaving a side area of 15.70 cm^2 exposed for testing. The coral aggregate and coral sand, as shown in Figs.1a and 1b, were adopted to prepare the CWC. The density and water absorption rate of the raw materials are presented in Tab. 1, and the size distribution of the coral sand was shown in Fig. 2.
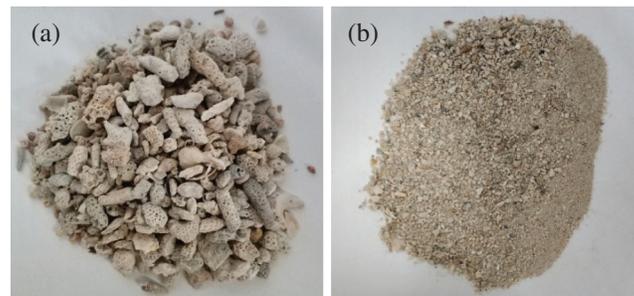
Figure 1: Photographs of the coral waste, (a) coral aggregate, (b) coral sands

Table 1: Physical properties of the coral

Materials	Bulk density (kg/m^3)	Apparent density (kg/m^3)	Water absorption rate (%)
Coral aggregate	939	1978	12.08
Coral sand	1286	2344	5.23

In order to improve the uniformity of the contained chlorides in the outdoor stored raw materials, the coral aggregate and coral sands were soaked into 3.5% (wt.%) NaCl solution before the preparation of the CWC. After 24 h, the coral was filtered from the solution and dried in the room temperature for five days. Thereafter, the coral aggregate and the coral sand were further dried in a drying oven at 80°C for 12 h. The tap water and 3.5% NaCl solution were used to prepare the OC and CWC, respectively. The corrosion characters of the two types of stainless steels (SS) in the seawater CWC with different strength grades, including C10, C20 and C30 were investigated. For comparison, the corrosion behavior of the CS in the C30 grade OC also was studied. The compositions of the CWC and OC samples, as well as the compressive strength and total porosity of the concrete samples at 28 days are presented in Tab. 2, in
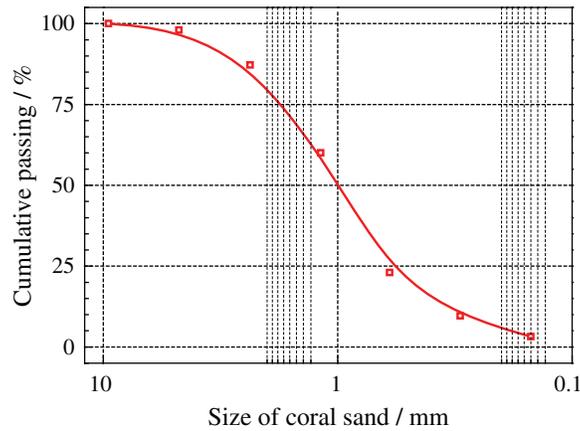
Figure 2: Size distribution of the coral sand applid in the CWC

Table 2: Compositions and mechanical properties of the CWC and OC

	CWC			OC	
Constituent	C10	C20	C30	Constituent	C30
Coral aggregate (kg/m^3)	721	658	647	Crushed stone (kg/m^3)	1243
Coral sand (kg/m^3)	504	460	453	River sand (kg/m^3)	532
Cement (kg/m^3)	350	400	440	Cement (kg/m^3)	440
Water (kg/m^3)	325	302	261	Water (kg/m^3)	185
W/c	0.93	0.75	0.59	w/c	0.42
Bulk density (kg/m^3)	1900	1820	1801	Bulk density (kg/m^3)	2400
Compressive strength (mpa)	13.4 ± 3.4	22.3 ± 2.5	28.7 ± 2.9	Compressive strength (mpa)	34.9 ± 2.7
Total porosity (%)	27.56	23.27	21.49	Total porosity at (%)	19.36

which the P.O 42.5 ordinary Portland cement was adopted. Firstly, the mixing solution in a ratio of 8% (wt.%) of the coral aggregate, was mixed with the aggregate for 1 min to pre-wet the latter material [23,24] and cement was mixed with the coral sand for 1 min. Thereafter, all the raw materials and the mixing solution were mixed for 3 min. The total weight of water relative to that of cement (wt.%) was defined as the water to cement ratio.

The steel rebar was embedded in the central of the cylindrical concrete, with a size of Φ100 mm × 80 mm, as shown in Fig. 3. Five samples were prepared for every condition. The mean values in
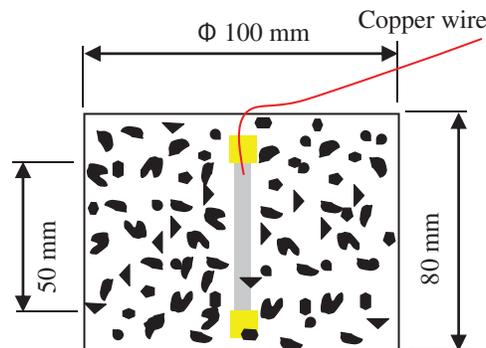
Figure 3: Illustration of the rebar in the concrete sample

potentials and polarization resistances were used while the middle ones in the EIS and the polarization curves were adopted. After being cured 24 h in the mold at room temperature, the samples were demolded and immersed in 3.5% NaCl solution.

2.2 Techniques

After the concrete samples were curing for 28 days, the compressive strength and the mercury intrusion porosimetry measurements were performed by applying an RE-8060 universal testing machine and an Auto Pore IV 9500 microparticle mercury porosimeter, respectively. A CS350 workstation was applied to conduct the electrochemical measurements. Polarization curves of the three types of steel in the pore solution without Cl^- and with 1.0 mol/L Cl^- were tested, for preliminarily verifying the potential of application of the SS in the CWC. The tests were carried out in a rate of 1.0 mV/s, began at -0.3 V $vs.$ OCP and stopped until the anodic current density higher than 1.0 mA cm^{-2}, after the samples were stabilized 2 h in the pore solutions. The polarization curve of the steel sample in the concrete was also tested with the aforementioned parameters after 750 days of immersion. Three-electrode arrangement was adopted in these electrochemical tests, in which a platinum plate was used as the counter electrode, a saturated calomel electrode (SCE) l was used as the reference electrode, and the steel sample was connected as the working electrode. For the concrete samples, open circuit potentials of the steel rebar were recorded when it changed less than 5 mV in 10 min after being connected. Linear polarization resistance (R_p) of the steel sample was measured from -15 mV to 15 mV $vs.$ OCP, at a scan rate of 0.1667 mV/s. Electrochemical impedance spectroscopies (EIS) of the steel samples were tested from 10^5 to 10^{-2} Hz, with a sinusoidal potential wave of 10 mV in amplitude around the OCP. Moreover, the corrosion state of the steel samples in the CWC and OC was examined at 750 d, after removing the concrete cover layer.

2.3 Ecological Evaluation of the Stainless Steel Reinforced CWC

The NREC and CE of the stainless steel reinforced CWC were compared with these of the carbon steel reinforced OC. As shown in Tab. 3, data of the NREC and CE of the raw materials from literatures [25–30] were used in this study. It is worth mentioning that the differences of NREC as well as CE between 2205SS and 304SS were ignored here. For the coarse aggregate, according to Chau et al. [30], the NREC and CE were in the range of 0.3–1.0 MJ/kg and 0.016–0.056 kg CO_2-e/kg, and they were chosen at 0.65 MJ/kg and 0.05 kg CO_2-e/kg, respectively. The CE of the CS rebar was selected as 2.7 kg CO_2-e/kg in the range of 1.03–3.51 kg CO_2-e/kg [30], and the NREC value of the SS rebar was 10.75 MJ/kg between 8.2 to 13.3 MJ/kg [29]. In addition, as Berndt [28] reported, the dosage of steel reinforcement in the concrete was 107.5 kg/m³ for the marine concrete structures. For the OC, the raw materials, like cement, river sand, coarse aggregate, CS rebar,

Table 3: NREC and CE of the raw materials

Materials	NREC (MJ/kg)	CE (kg/kg)	Source
P.O 42.5 cement	5.75	0.85	[1]
river sand	2.24×10^{-2}	1.06×10^{-3}	[1]
coarse aggregate	0.65	0.05	[30]
CS rebar	8.6	2.7	[26,30]
stainless steel rebar	10.75	3.38	[29,30]
fresh water	0	0	[1]
seawater	0	0	
coral waste	0	0	[1]

as well as the fresh water should be transported from the mainland, and a distance of 1200 km was adopted, same to that in the earlier literature [1]. On the other hand, for the SS reinforced CWC, only the SS reinforcement and cement need to be transported from the mainland because the coral waste and seawater can be obtained on the islands. The NREC and CE of shipping are 0.13 MJ.Km^{-1} T^{-1} and 0.0089 kg Km^{-1} T^{-1}, respectively [2]. According to the aforementioned data and the compositions of the CWC and OC shown in Tab. 1, the NREC and CE of each cubic meter of the newly constructed SS reinforced CWC as well as CS reinforced OC on the island far from the mainland was calculated.

Furthermore, the design life of the marine harbor is 50 years in China [31]. In the present study, the NREC and CE of the SS reinforced CWC and CS reinforced OC also were assessed on the tropical island condition in a duration of 50 years. In fact, there is lacked of the inspection data of the SS reinforced CWC on the tropical island. Recently, Yu et al. [32] investigated the corrosion state of carbon steel reinforced concrete structures located in the South China Sea, and they noticed that the 20-year structures were obviously corroded. In addition, one earlier study [33] also suggested that the first repair of the CS reinforcement concrete in marine environement should be conducted at 10 years after its construction. In the present study, the safe time (the time before corrosion initiation) of the CS-C30 OC is assumed to be 10 years. For i_{corr} of the SS-C30 CWC in less than one-tenth of that of the CS-C30 OC counterpart, the safe time of the former concrete structure should be longer than 100 years, and the SS-C30 CWC don't need to be repaired in the 50 years duration. In fact, the reasonability of this assumption could be confirmed by the corrosion performance of the Progreso pier. Many studied [34,35] have reported that the Progreso pier, which is the first stainless steel reinforced concrte structure, in Yucatan, did not exhibit any visible corrosion after serving more than 60 years without any major maintenance [35]. For the CS-C30 OC, same to earlier studies [33,35], the structure needs 10%, 15%, and 20% repair at the 10th year, 25th year, and 40th year after being constructed, respectively, as shown in Tab. 4. Finally, the NREC and CE of the maintenance in 50-year duration were also estimated basing on the data of the raw materials and transportion. The demolition and construction were excluded for the lack of reliable data [35].

Table 4: The maintain of the CS-C30 OC and SS-C30 CWC in 50-year duration [33,35]

	10th year	25th year	40th year	50th year	Waste
CS-C30 OC	10% repair	15% repair	20% repair	rebuild	100%
SS-C30 CWC		No repair			Zero

3 Results and Discussion

3.1 Polarization Curves in the Pore Solution

Fig. 4 shows the polarization curves of the three types of steels in the simulated concrete pore solutions without Cl^{-} as well as with 1.0 mol/L Cl^{-}. Clearly, the anodic current density of the CS exhibits the highest value, while that of the 2205SS presents the lowest value among the three types of steels in the same pore solutions. Furthermore, in comparison to the anodic current densities of the samples in the solution without Cl^{-}, those of the ones in the chloride-containing solutions (1.0 mol/L) were significantly enhanced. Especially, the current density of the CS almost was increased by two orders of magnitude when a concentration of 1.0 mol/L Cl^{-} was added into the simulated pore solution, while the anodic current densities of the two stainless steels were enhanced no more than one order of magnitude. The corrosion current densities (i_{corr}) of steel samples in the pore solutions were further calculated from the polarization curves. As Fig. 5 shows, the i_{corr} of the two types of stainless steel in the chloride-containing solution (1.0 mol/L) are even lower than that of the CS counterparts in the chloride-free solution. Similarly, Alvarez et al. [36] compared the corrosion resistance of CS, 304SS, as well as 2205SS in the carbonated
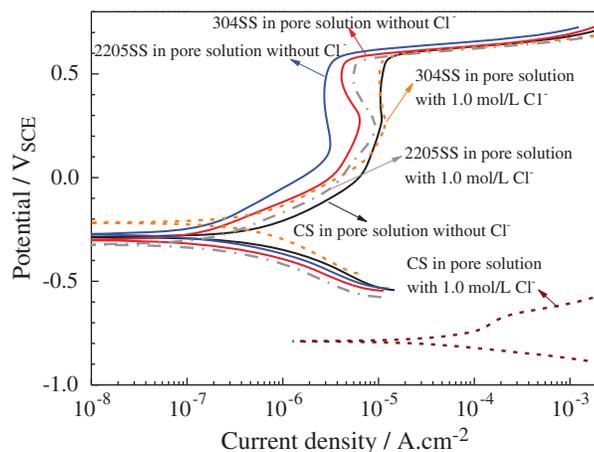
Figure 4: Polarization curves of the three types steel in the simulated concrete pore solution without Cl$^-$ and the pore solution containing 1.0 mol/L NaCl after being stabilized 2 h, respectively
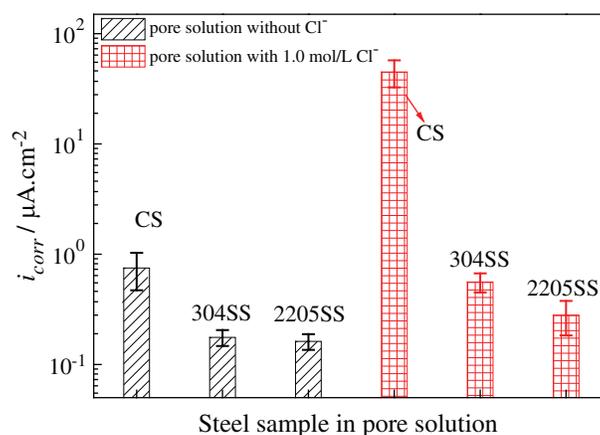
Figure 5: The i_{corr} calculated from the polarization curves of the three types steels in the simulated concrete pore solutions after being stabilized 2 h

and non-carbonated pore solutions, respectively. The results indicated that the i_{corr} of the stainless steels in the pore solution contaminated 5.0 % Cl$^-$ was still slightly lower than that of the CS in the Cl$^-$-free pore solutions. This scenario suggests that the application of the stainless steel reinforcement in the CWC is one of the candidate ways to solve its durability issue.

3.2 Open-Circuit Potential in the CWC

Fig. 6 displays the OCP values of the steel samples in the seawater CWC as well as the OC. The potentials of the steel reinforcement negatively shifted in the initial 100 d, then the values of OCP obviously increased from 100 d to 200 d. Thereafter, the OCP maintained at a relatively stable value in the following 150 d, and its gradually decreased again after 400 d of immersion in the 3.5% NaCl solution. The decrease of potentials at the beginning could be ascribed to the Cl$^-$ included in the mixing water, coral sand, and coral aggregate, as well as to the rapid migration of the Cl$^-$ from the solution into the early-aged high porosity concrete for its low achieved degree of hydration [37]. With time increasing, the cementitious materials in the concrete gradually hydrated and the pores of the concrete were filled with the production of the hydration reaction. The migration of the Cl$^-$ from the solution into the concrete
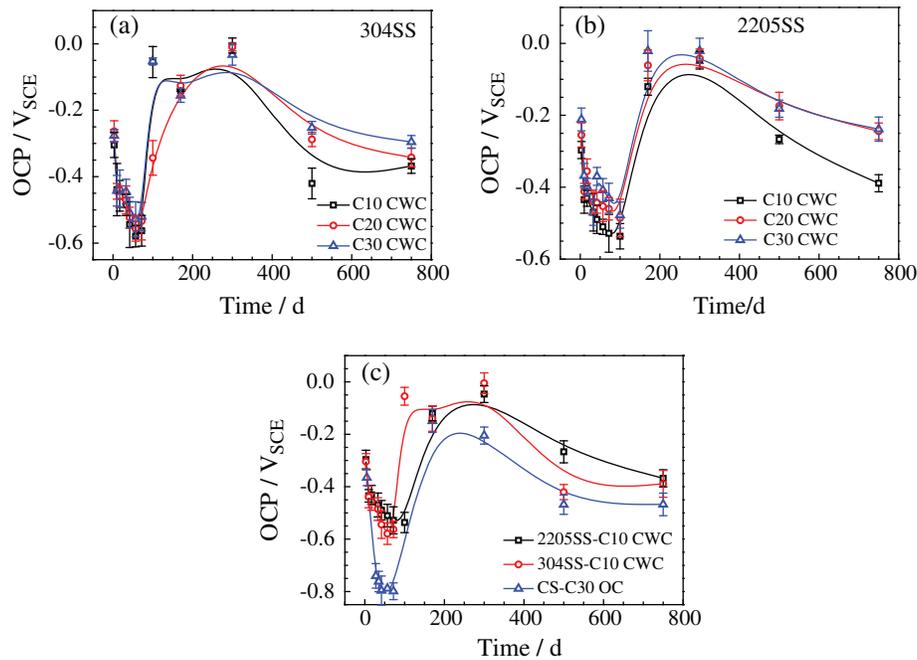
Figure 6: OCP of the three types of steel reinforcement in different grades CWC as well as OC

was hindered. Simultaneously, the production of hydration reaction, calcium hydroxide ($Ca(OH)_2$), increased the surrounding pH of the steel reinforcement [38], leading to the rebar repassivation. Consequently, as Fig. 6 shows, the values of OCP increased with time from 100 d to 200 d. As time further increased, more aggressive ions migrated to the concrete/rebar interface and caused the degradation of the passive films, which gave rise to another decrease in OCP after 400 d. Similarly, Bertolini et al. [39] investigated the corrosion behavior of two types of low-nickel stainless steel (2304 and 2101) in the chloride contaminated concrete. The corrosion potentials of the steels also decreased with time in the initial one month, then gradually increased in the following four months, and decreased again five months later. In addition, as shown in Figs. 6a and 6b, the potentials of the two stainless steels evidently increased with the strength grade of the CWC, but no significant difference in the OCP of the two stainless steels can be observed in the CWC. Moreover, the potential of the two types of stainless steel reinforcements in a low strength grade CWC (C10) is even obviously more positive than that of the CS counterpart in a high strength grade OC (C30), indicating the high corrosion resistance of the stainless steel in the CWC.

3.3 Liner Polarization Resistance in the CWC

According to ASTM G 59–91 [40], the R_p of the SS and CS in the CWC and OC, as well as the corresponding i_{corr} was determined as follows:

$$R_P = \left(\frac{\Delta E}{\Delta i}\right)_{\Delta E \to 0} \tag{1}$$

$$i_{corr} = \frac{\beta_\alpha \beta_c}{2.303 R_P (\beta_c - \beta_\alpha)} \tag{2}$$

$$B = \frac{\beta_\alpha \beta_c}{2.303(\beta_c - \beta_\alpha)} \tag{3}$$

$$i_{\text{corr}} = \frac{B}{R_P} E = mc^2 \tag{4}$$

where E is the applied potentials around the OCP, i is the current density, β_α represents the anodic Tafel slopes, and β_c represents the cathodic Tafel slopes, on a log scale [41]. According to the earlier studies [42–44], β_α was 90 mV/dec, β_c was -180 mV/dec for the CS rebar in concrete, and $B = 26$ mV/dec is used for the CS here. For the stainless steel samples, same to previous studies [39,45–48], $B = 26$ mV was employed to calculate its i_{corr}. Furthermore, the corrosion rates of reinforcing steel in concrete were categorized into four grades by the values of i_{corr}, as shown in Fig. 7, according to Otieno [49] and Broomfield [50].
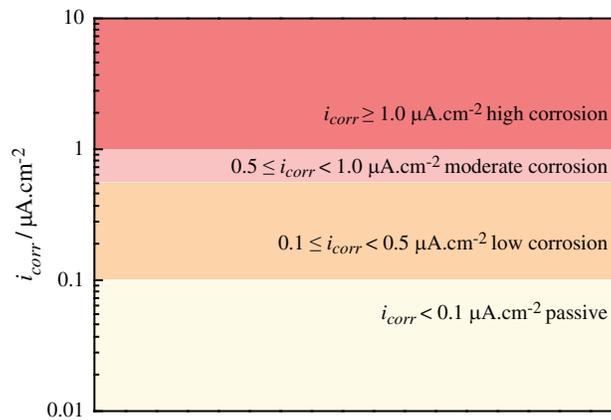
Figure 7: Corrosion state of rebar in concrete was categorized into four grades by the i_{corr} [49,50]

Fig. 8 presents the R_p and its corresponding i_{corr} of the steel sample in the CWC as well as the OC. Clearly, the R_p of the SS samples in the CWC obviously increased with time, while that of the CS in the OC just slightly increased as time extended. Thus, the corresponding i_{corr}, as displayed in Figs. 8b, 8d, and 8f, generally decreased with time. The i_{corr} of the two types of SS in the CWC are in the range of 0.01–0.07 µA cm^{-2}, while that of the CS in the C30 OC is of the magnitude of several µA cm^{-2}. According to the i_{corr} standard shown in Fig. 7 [49,50], both 304SS and 2205SS in the CWC could be categorized as the passive state during the whole experimental period, while the CS counterpart in the C30 OC was categorized as the high corrosion state in the initial 400 d and gradually changed to the low corrosion state in the following time.

In addition, the i_{corr} of the two SS reinforcements in the C10 CWC is almost two orders of magnitude lower than that of the CS counterpart in the C30 OC, as shown in Fig. 8f, revealing that the corrosion resistance of the SS reinforced CWC is much higher than that of the CS reinforced OC. In an earlier study, García-Alonso et al. [47] compared the corrosion behavior of the 304SS, low-Ni austenoferritic stainless steel (HSS2), and CS in the chloride-containing (4.0% by weight of cement) high-performance concrete (HPC, C60/C70 grade), and they reported that the i_{corr} of the three steels, are around 0.01 µA cm^{-2}, 0.3–0.8 µA cm^{-2}, and 0.7–10 µA cm^{-2} (Fig. 8), respectively. In comparison, the 304SS and 2205SS in the CWC (C10~C30) exhibit the higher i_{corr} than that of the 304SS in the chloride-containing HPC (C60/C70). However, the i_{corr} of the former two SS reinforcements in the CWC is almost one order of magnitude lower than that of the low-Ni austenoferritic stainless steels (HSS2) in Cl$^-$ contaminated HPC at 800 d, while García-Alonso et al. [47] suggested that the HSS2 stainless steel reinforcement has
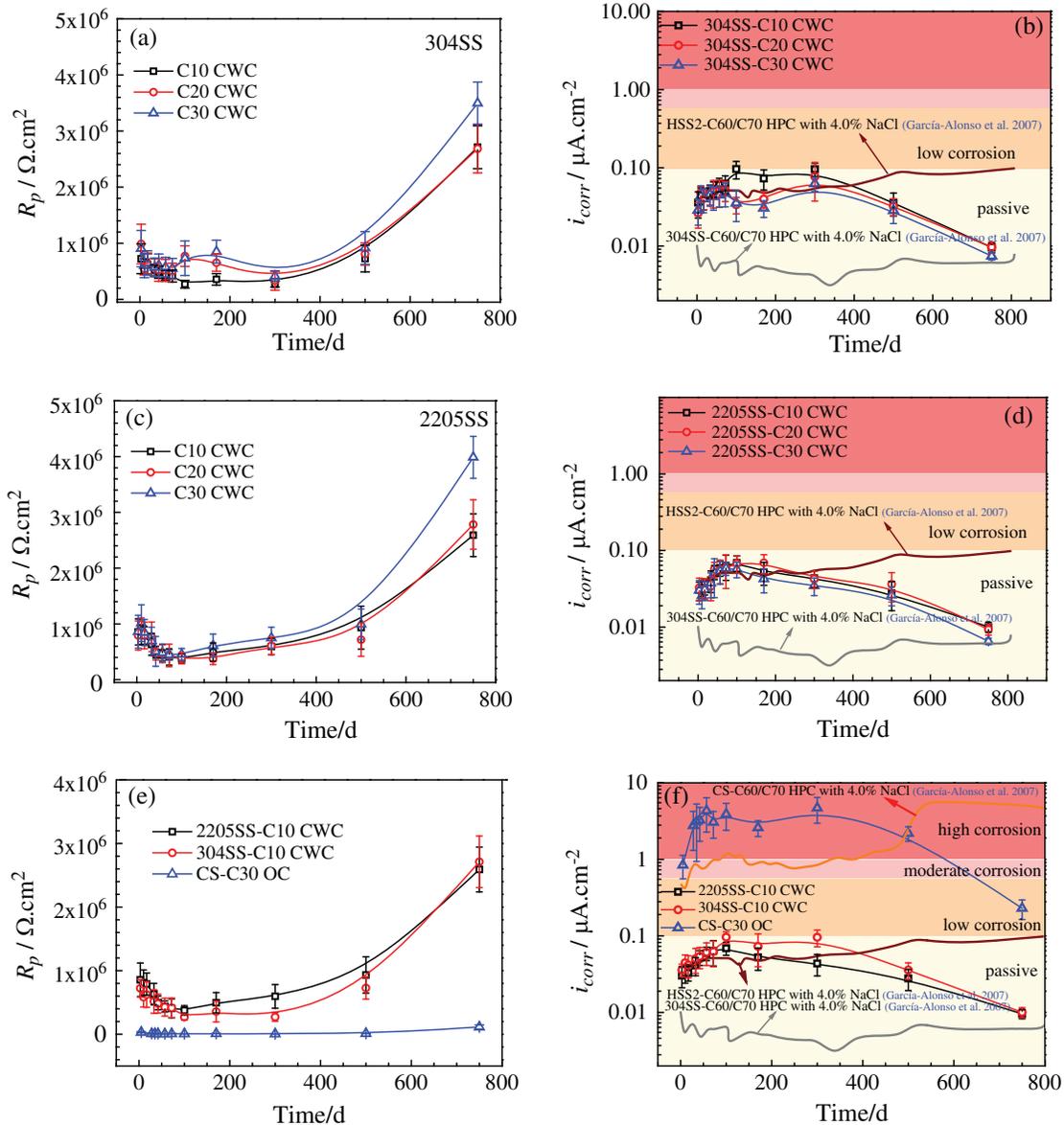
Figure 8: The R_p and the corresponding i_{corr} of the steel samples in concrete, (a) and (b) 304SS in the CWC, (c) and (d) 2205SS in the CWC, (e) and (f) the two types of stainless steel in the C10 CWC as well as the CS in the C30 OC

adequate corrosion resistance in the Cl⁻ contaminated HPC (C60/C70). This scenario further confirms that the durabilities of the 304SS and 2205SS reinforced CWC are satisfying. Simultaneously, the i_{corr} of the 2205SS is slightly lower than that of the 304SS in the same grades CWC, as shown in Fig. 8f, which is consistent with the earlier study conducted by Alvarez et al. [36], indicating the higher corrosion resistance of the former stainless steel.

3.4 Electrochemical Impedance Spectroscopy in the CWC

Fig. 9 shows the EIS results of the steel samples in the CWC and OC. Obviously, the capacitive loop radius of the CS sample in the high strength grade OC (C30) is always smaller than those of the SS
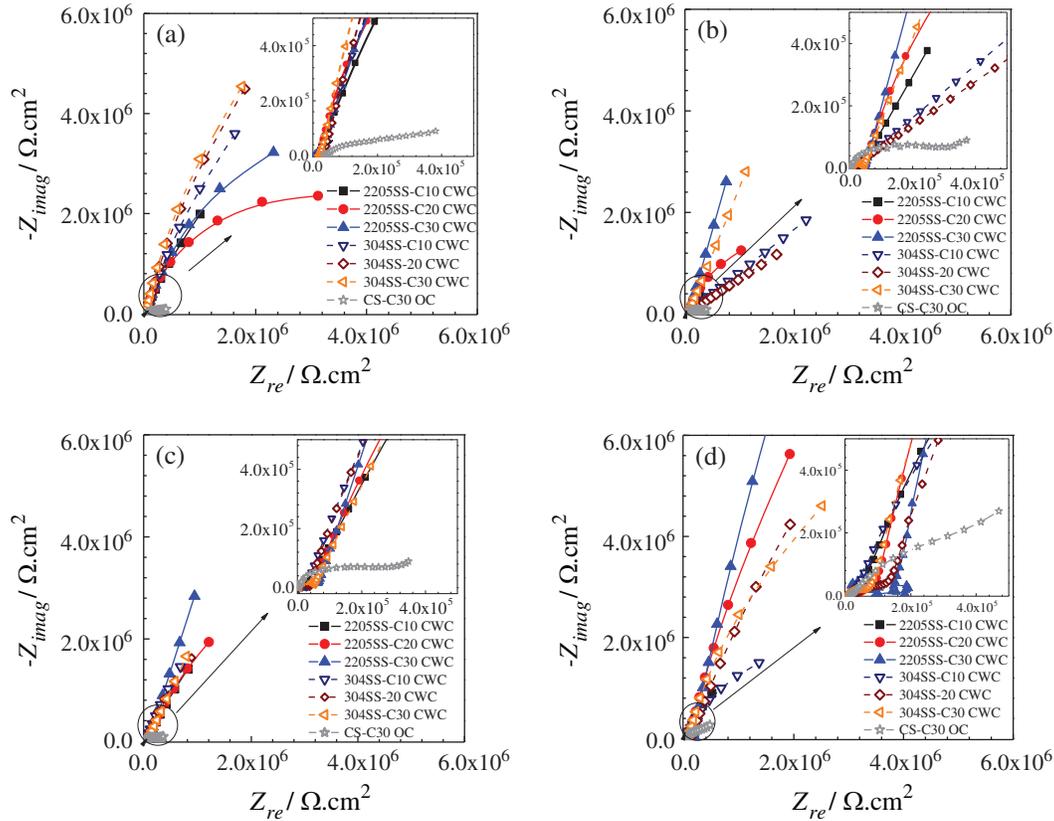
Figure 9: Nyquist plots of two types of stainless steels in the CWC as well as the CS in the OC at different time. (a) 34 d, (b) 170 d, (c) 300 d, (d) 750 d

counterparts in the low strength grade (C10) CWC. This scenario, together with the OCP (Fig. 6) and LPR (Fig. 8) results, suggests that the two types of SS reinforcements in the CWC presented the higher corrosion resistance than that of the CS counterpart in the OC. Simultaneously, except at 34 d, the capacitive loop radius of the 2205SS samples are always larger than those of the 304SS ones in the same strength grade CWC, indicating the higher corrosion resistance of the former SS reinforcement.

The equivalent electrical circuit [51–55] shown in Fig. 10, was introduced to further analyze the EIS data, where R_s is the solution resistance; R_{con} is the concrete resistance and CPE_{con} is the concrete capacitance; CPE_{ct} is the capacitive behavior of the double layer capacitance, and R_{ct} is the polarization resistance [51–55]. As widely used in EIS data fitting in previous studies [51–55], the constant phase element (CPE) was applied to replace the pure capacitance. The impedance of Z_{CPE} is defined as follows [51–55]:

$$Z_{CPE} = Y_0^{-1}(jw)^{-n} \tag{5}$$

where Y_0 is the capacitance value of CPE, w represents the angular frequency, j represents the imaginary number, n, named as the CPE exponent, was in the range from 0 to 1, which reflects the degree of deviation from the ideal capacitance. When $n = 1$, it means that the CPE is a pure capacitance, while $n = 0$, the CPE becomes a pure resistance [52,54,55]. The values of n is in the range from 0.6 to 0.9 in the present study.
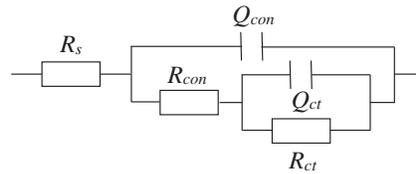
Figure 10: Equivalent electrical circuit used for modelling of the impedance data

As Fig. 11 shows, the equivalent circuit excellently fits the experimentally tested EIS data, and the fitted results are presented in Fig. 12. The R_{con} of C30 OC is apparently higher and its CPE_{con} is obviously lower than those of the CWC counterparts with the same strength grades, which is consistent with the tested total porosity results (Tab. 2). Simultaneously, the R_{con} of the CWC increased with the strength grade. For instance, for the 304SS samples, the R_{con} values of the C30 CWC is obviously higher than that of the C10 samples, which should be ascribed to the porous structure of coral aggregate. In order to produce high strength CWC, both the contents of coral aggregate and coral sand decreased while the content of cement increased (Tab. 1). The total porosity of the CWC diminished (Tab. 2) and the compactness of the concrete increased with the strength grade. Consequently, the R_{con} increased with the strength grade in the CWC. Meanwhile, since the crushed stone aggregates have the more compact microstructure than the coral aggregates, the R_{con} value of the OC is significantly higher and its CPE_{con} is obvious lower than those of the CWC counterparts even with the same strength grade, as shown in Figs. 12a and 12c. The fitted R_{ct} of the CS
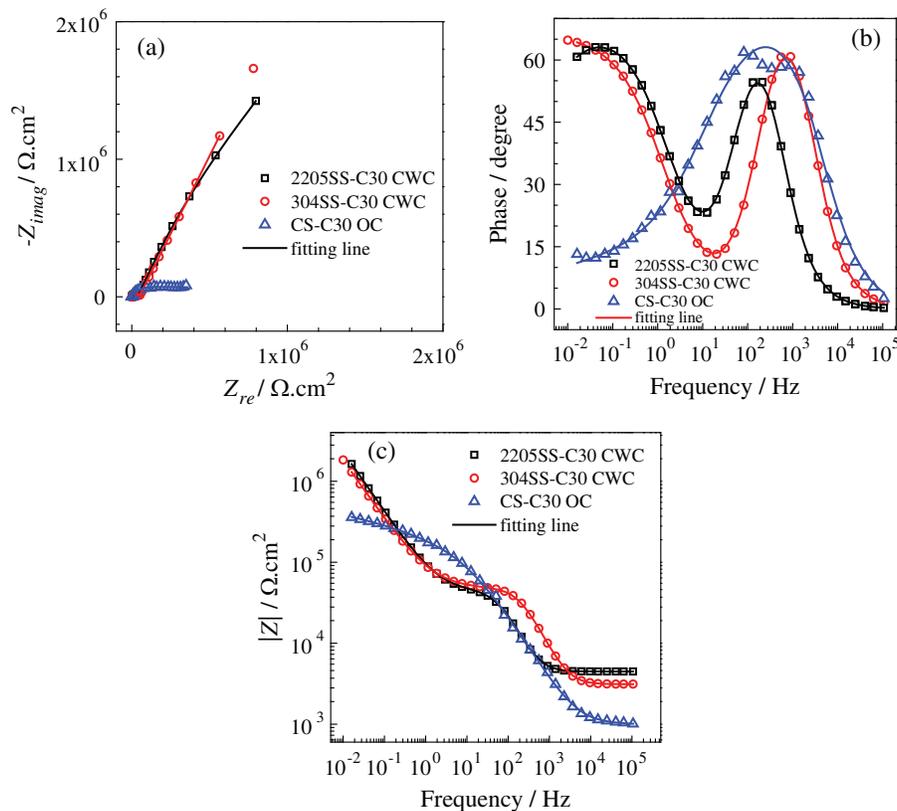
Figure 11: The experimental and fitted EIS results of the steel samples in the CWC and OC after being immersed in the 3.5% NaCl solution for 300 d
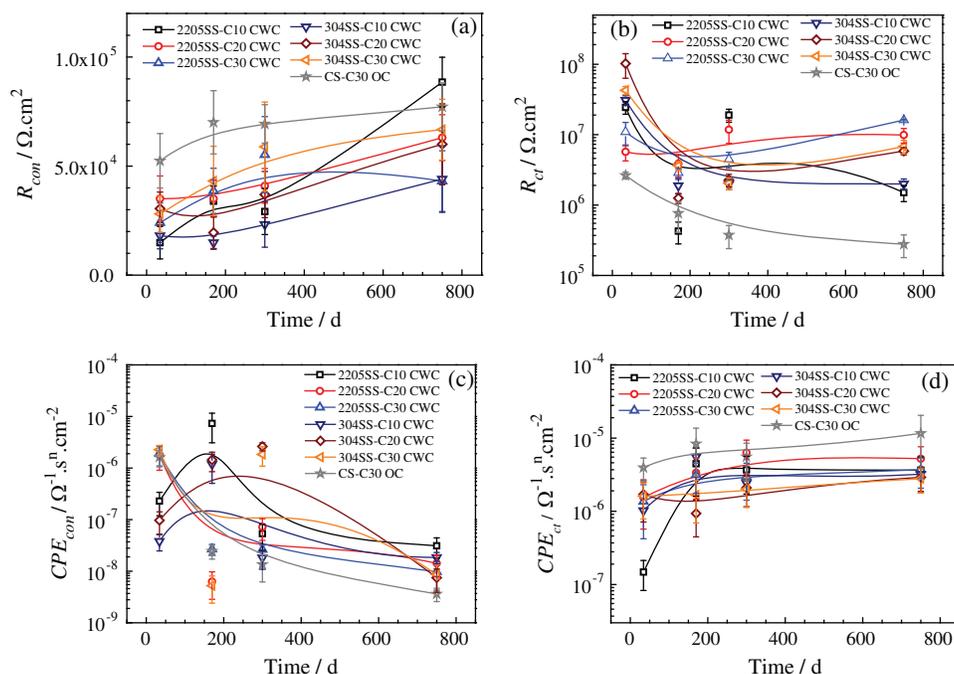
Figure 12: Fitted results in EIS data of the steel reinforcement in concrete at different time, (a) the concrete cover layer resistance (R_{con}), (b) the polarization resistance (R_{ct}), (c) the concrete capacitance (CPE_{con}), CPE_{con} is the concrete capacitance; (d) the double layer capacitance (CPE_{ct})

in the high strength grade OC (C30) is one order of magnitude lower, and its corresponding CPE_{ct} is significant lower than those of the SS counterparts in the low strength grade CWC (C10), as shown in Figs. 12b and 12d, which should be related to the different passivity of the CS and SS in the concrete environment.

The i_{corr} of the steel samples in the concrete also were calculated through Stern and Geary's equation from the fitted R_{ct}, in which $B = 26$ mV is employed [39,45–48], and the results are displayed in Fig. 13. Obviously, the CS in the high grade OC (C30) exhibits the highest i_{corr}, and the i_{corr} of the 304SS is higher than that of the 2205SS in the same grade CWC. This scenario is consistent with previous studies
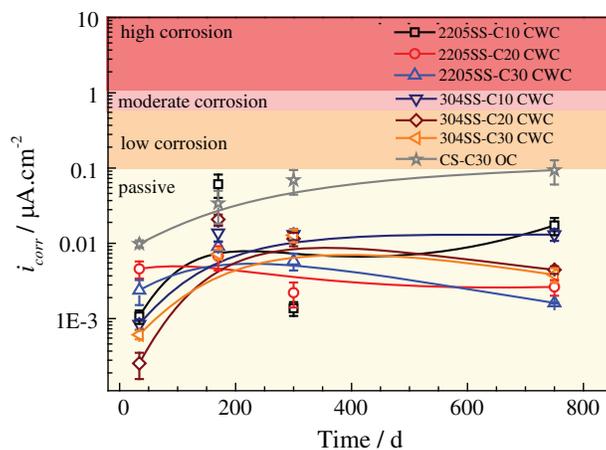
Figure 13: The i_{corr} of the steel samples in the CWC and OC calculated from the fitting polarization resistance (R_{ct}) in EIS data

[39,45–48], confirming that the passive current densities of the steels in the concrete depends on the types or the grades of steel. Furthermore, in comparison to the i_{corr} calculated from the linear polarization resistance (Fig. 8), the i_{corr} got from the R_{ct} in EIS data (Fig. 13) is much low. In fact, an earlier study conducted by Pech-Canul et al. [56] also indicated the discrepancy in i_{corr} from the aforementioned two technologies, and they ascribed it to the uncertainties typical of electrochemical measurements in passive systems [57]. Moreover, according to the i_{corr} standard shown in Fig. 7 [49,50], all the steel reinforcements in the concrete should be defined as the passive state because the value of i_{corr} is lower than 0.1 μA cm^{-2}, as shown in Fig. 13.

3.5 Polarization Curves in the CWC

Fig. 14 presents polarization curves of the steel reinforcement in the CWC and OC after 750 d of immersion. Obviously, the anodic current density of the CS immersed in the C30 OC is highest, while that of the 2205SS in the same grade CWC is the lowest. Simultaneously, the anodic current density of the 2205SS is always lower than that of their 304SS counterpart in the same grade CWC, which is in line with the i_{corr} results in the pore solution (Figs. 4 and 5). In addition, the i_{corr} of the steel reinforcements in the concrete were calculated from the polarization curves in Fig. 14, and the results are displayed in Fig. 15. All the value of i_{corr} are less than 0.1 μA cm^{-2} after 750 d of immersion in the 3.5% NaCl solution, suggesting that the steel reinforcement in the CWC as well as OC maintained passivation according to the i_{corr} standard [49,50] (Fig. 7). Meanwhile, the i_{corr} of the two types of SS reinforcements in the CWC are much lower than that of the CS in the OC. Especially, when the grade of the CWC is same to the OC, the i_{corr} of the SS is even less than one-tenth of their CS counterpart.
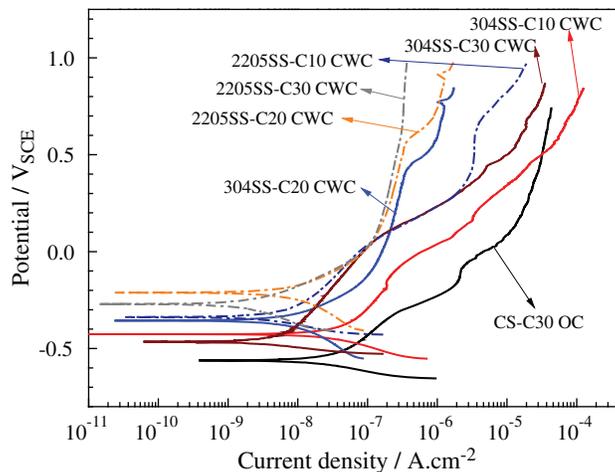
Figure 14: Polarization curves of the three types of steels in the CWC and OC at 750 d

3.6 Corrosion of the Steel Samples in the CWC

The concrete cover layers were removed, and the corrosion state of the steel reinforcement was examined at 750 d. As displayed in Fig. 16, the CS immersed in the C30 OC was severely corroded (Fig. 16a) while these stainless steel reinforcements in the CWC did not show any visible corrosion sites except the 304SS sample immersed in the C10 CWC (Fig. 16b). Furthermore, the cross-section of the corroded steel reinforcement (the arrows pointed in Fig. 16), the 304SS in the C20 CWC, and the 2205SS in the C10 CWC also were inspected. The CS immersed in the C30 OC and the 304SS in the C10 CWC were separately corroded more than 100 μm (Fig. 17a) and ~10 μm (Fig. 17b) in the depth direction, while the other stainless steel reinforcements do not exhibit obvious corrosion sites at the
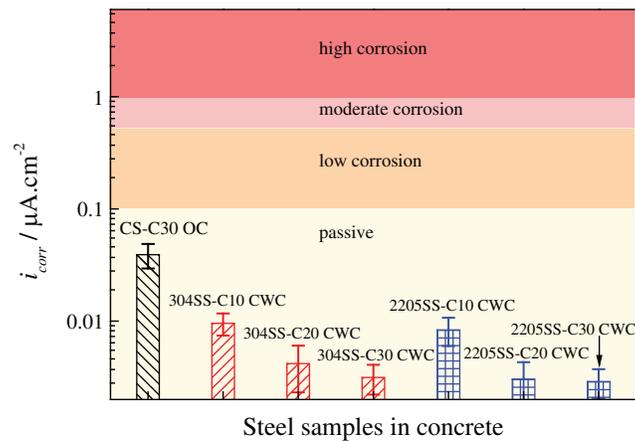
Figure 15: The i_{corr} of the steel samples in the CWC and OC at 750 d, calculated from the polarization curves
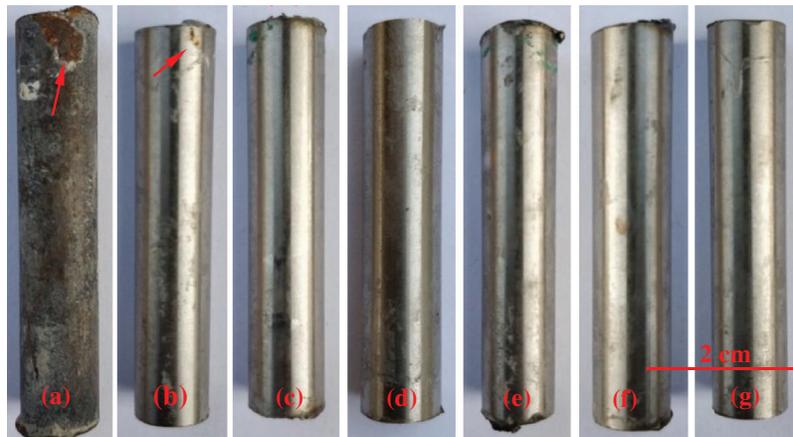
Figure 16: Corrosion state of the steel samples in the CWC and OC at 750 d, (a) CS in C30 OC, (b) 304SS in C10 CWC, (c) 304SS in C20 CWC, (d) 304SS in C30 CWC, (e) 2205SS in C10 CWC, (f) 2205SS in C20 CWC, (g) 2205SS in C30 CWC

cross-section (Figs. 17c and 17d). This situation confirms that it is satisfying that the durabilities of the stainless steel reinforced CWC samples and especially the 2205SS reinforced.

Furthermore, the i_{corr} of the three types of steel in the CWC and OC were calculated from the LPR, EIS, and polarization curves, respectively. According to the i_{corr} standard proposed by Otieno [49] and Broomfield [50], all the steel reinforcements maintained passivation in the CWC and the OC basing on the EIS (Fig. 13) and the polarization curves (Fig. 15) results. However, the i_{corr} calculated from the LPR (Fig. 8) suggested that the CS in the C30 OC was in the high or moderate corrosion state, while their SS counterparts immersed in the CWC were in the passive state. In general, the observed corrosion state of the steel reinforcements in the concrete (Figs. 16 and 17) is most consistent with the i_{corr} calculated from the LPR. In an earlier study, Poursaee et al. [58] systematically compared the corrosion rates of the reinforcing steel in concrete via potentiostatic linear polarization resistance, galvanostatic pulse polarization, electrochemical impedance spectroscopy, potentiodynamic cyclic polarization, and galvanodynamic polarization. Futhermore, they compared these corrosion rates with that from the mass loss. The results displayed that the potential-applied methods are more reliable than the current-applied
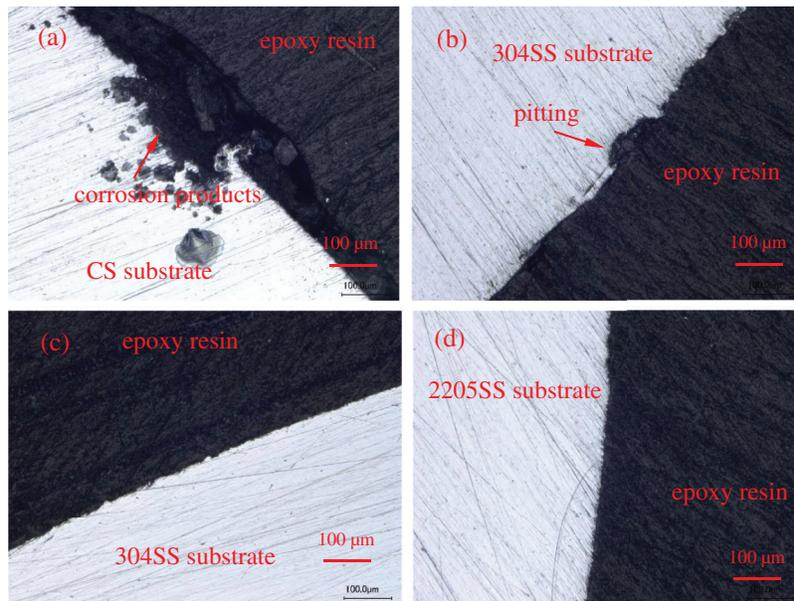
Figure 17: Optical micrographs of the cross-section of the steel reinforcement in the concrete after 750 d, (a) CS in C30 OC, (b) 304SS in C10 CWC, (c) 304SS in C20 CWC, (d) 2205SS in C10 CWC

ones, and the potentiostatic LPR method was proposed to be applied for the corrosion rate measurement of the steel reinforcement in concrete. Consequently, the corrosion current density results (Figs. 8, 13, and 15), together with the results reported by Poursaee et al. [58], confirm that the potentiostatic LPR is the most suitable technology to test the corrosion rate of the steel reinforcement in the CWC.

3.7 Ecological Evaluation of the Stainless Steel Reinforced CWC

It was calculated that the NREC and CE of per cubic metre of the newly constructed stainless steel reinforced CWC and carbon steel reinforced OC on the tropical island, as shown in Fig. 18. Clearly, for the SS reinforced CWC, both the NREC and CE of the raw materials as well as the transportion increased with the strength grade of the CWC. In addition, the NREC and CE of the SS reinforced CWC were mostly introduced in the product process of the raw materials, in which the NREC accounts for more than 97.7% while the CE is higher than 99.2%. Comparing the SS reinforced CWC (SS-C30 CWC) to the CS reinforced OC (CS-C30 OC) with the same grade, the NREC and CE of the latter material in the transportation are 4.65 times and 4.58 times of those of the former one, and the total NREC and CE of per cubic metre of SS-C30 CWC were 23.72% and 1.419% less than those of the CS-C30 OC. Meanwhile, per cubic meter of the newly constructed SS-C30 CWC saves 1243 kg natural aggregate, 532 kg river sand, and 185 kg fresh water in comparison to the CS-C30 OC counterpart. Furthermore, the NREC and CE of per cubic metre of SS-C30 CWC and CS-C30 OC in 50-year duration were calculated and results are displayed in Fig. 19. Both the NREC and CE of the CS-C30 OC increased with time, while those of the SS-C30 CWC did not show obvious change. Since the CS-C30 OC needs to be repaired three times, the SS-C30 CWC reduces 44.81% NREC and 32.0% CE than the CS-C30 OC counterpart in the 50-year duration, respectively. Meanwhile, per cubic meter of the CS-C30 OC would consume much natural resources, like 1802 kg coarse aggregate, 771 kg river sand, and 268 kg fresh water from the mainland in 50-year duration, while the SS-C30 CWC counterpart was prepared by adopting the coral waste and seawater on the island. This scenario suggests the stainless steel reinforced CWC is one type of cleaner as well as high-durable structure on these islands far from the mainland.
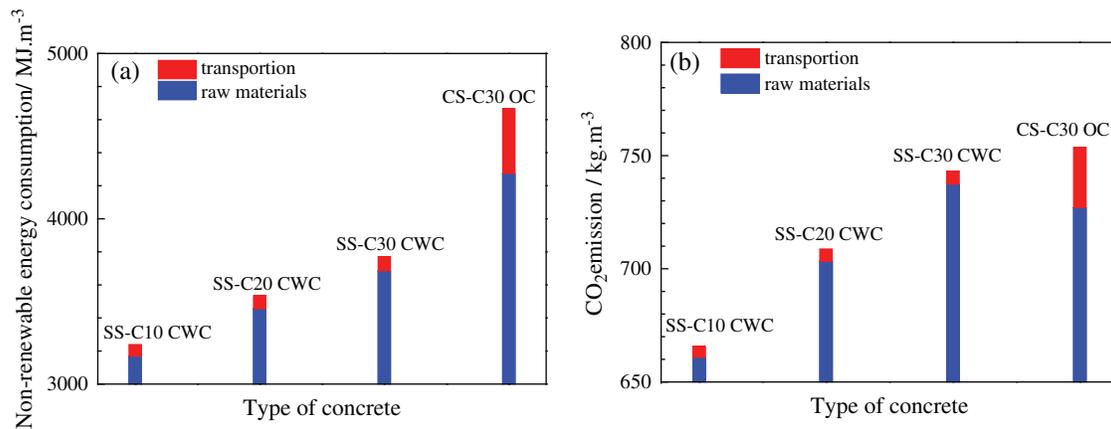
Figure 18: Ecological evaluation of per cubic meter newly constructed SS reinforced CWC and CS reinforced OC, (a) NREC, (b) CE
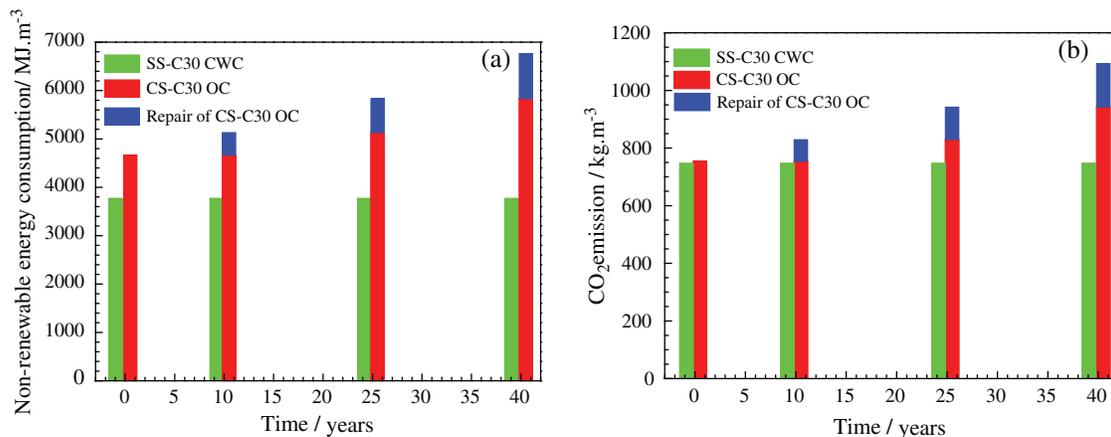
Figure 19: Ecological evaluation of per cubic meter of SS-C30 CWC and CS-C30 OC in 50 years duration, (a) NREC, (b) CE

4 Conclusions

Corrosion resistances of the 304SS and 2205SS in the CWC was compared to that of the CS in the OC in 3.5% NaCl solution with the OCP, LPR, EIS, and polarization curves. It was calculated that the NREC and CE of per cubic meter of newly constructed SS-C30 CWC and CS-C30 OC and the evolution of the NREC and CE in 50-year duration was deduced. The following conclusions were drawn from the results.

(1) The i_{corr} of the 304SS and 2205SS reinforcements in the CWC decreased with the concrete strength grade, and the i_{corr} of the latter steel was lower than that of the former one in the same grade CWC.

(2) In comparison, the i_{corr} of the two types of SS reinforcement in the CWC was obviously lower than that of the CS counterpart in the OC, and the i_{corr} of the SS reinforcement was less than one-tenth of the latter one when the CWC and OC with the same strength grade.

(3) The two SS reinforcements in the CWC exhibited passive states even after being immersed in 3.5% NaCl solution for more than two years. Thus, the application of the stainless steel, especially the 2205SS reinforcements, should be one of the effective ways to enhance the durability of the CWC structure.

(4) The i_{corr} calculated from the LPR data is most consistent with the observed corrosion state results. Hence, the LPR method was proposed to measure the corrosion rate of the steel reinforcement in the CWC.

(5) Per cubic meter of newly constructed SS-C30 CWC reduces 23.72% NREC and 1.419% CE compared to the CS-C30 OC counterpart, and the NREC and CE of the former material would be diminished 44.81% and 32.0% than those of the latter one in 50-year duration, for the three times of repair of the CS-C30 OC. Therefore, the stainless steel reinforced coral waste concrete is a clean construction material with high durability on the island far from the mainland.

Conflicts of Interest: The authors declare that they have no conflicts of interest to report regarding the present study.

References

1. Wang, Y., Shui, Z., Gao, X., Huang, Y., Yu, R. et al. (2019). Utilizing coral waste and metakaolin to produce eco-friendly marine mortar: hydration, mechanical properties and durability. *Journal of Cleaner Production, 219,* 763–774. DOI 10.1016/j.jclepro.2019.02.147.

2. Bundesverband Der Deutschen Ziegelindustrie, E. V. E. (2017). *Green Building Challenge Handbuch.* (Accessed 12 October 2017).

3. Arumugam, R. A., Ramamurthy, K. (1996). Study of compressive strength characteristics of coral aggregate concrete. *Magazine of Concrete Research, 48(176),* 141–148. DOI 10.1680/macr.1996.48.176.141.

4. Kakooei, S., Akil, H. M., Dolati, A., Rouhi, J. (2012). The corrosion investigation of rebar embedded in the fibers reinforced concrete. *Construction and Building Materials, 35,* 564–570. DOI 10.1016/j.conbuildmat.2012.04.051.

5. Wang, Q., Li, P., Tian, Y., Chen, W., Su, C. (2016). Mechanical properties and microstructure of Portland cement concrete prepared with coral reef sand. *Journal of Wuhan University of Technology-Materials Science Edition, 31 (5),* 996–1001. DOI 10.1007/s11595-016-1481-x.

6. Cheng, S., Shui, Z., Sun, T., Yu, R., Zhang, G. et al. (2017). Effects of fly ash, blast furnace slag and metakaolin on mechanical properties and durability of coral sand concrete. *Applied Clay Science, 141,* 111–117. DOI 10.1016/j.clay.2017.02.026.

7. Wu, W., Wang, R., Zhu, C., Meng, Q. (2018). The effect of fly ash and silica fume on mechanical properties and durability of coral aggregate concrete. *Construction and Building Materials, 185,* 69–78. DOI 10.1016/j.conbuildmat.2018.06.097.

8. Liu, J., Ou, Z., Peng, W., Guo, T., Deng, W. et al. (2018). Literature review of coral concrete. *Arabian Journal for Science and Engineering, 43(4),* 1529–1541. DOI 10.1007/s13369-017-2705-x.

9. Wang, L., Wang, G. X., Deng, X. L. (2014). Research on the mechanical properties of different content carbon fiber coral concrete. *China Rural Water and Hydropower, 9,* 148–156 (in Chinese).

10. Wang, L., Yi, J., Deng, X. L., Li, J. Y. (2016). Study on mechanical property and damage morphology analysis of coral aggregate concrete with fiber. *Journal of Henan Polytechnic University (Natural Science), 35,* 713–718 (in Chinese).

11. Yoo, D. Y., Banthia, N. (2016). Mechanical properties of ultra-high-performance fiber-reinforced concrete: a review. *Cement Concrete Composites, 73,* 267–280. DOI 10.1016/j.cemconcomp.2016.08.001.

12. Mo, K. H., Alengaram, U. J., Jumaat, M. Z. (2016). Structural performance of reinforced geopolymer concrete members: a review. *Construction and Building Materials, 120,* 251–264. DOI 10.1016/j.conbuildmat.2016.05.088.

13. Wang, A., Lyu, B., Zhang, Z., Liu, K., Xu, H. et al. (2018). The development of coral concretes and their upgrading technologies: a critical review. *Construction and Building Materials, 187,* 1004–1019. DOI 10.1016/j. conbuildmat.2018.07.202.

14. Ehlert, R. A. (1991). Coral concrete at Bikini Atoll. *Concrete International, 13,* 19–23.

15. Hurley, M. F., Scully, J. R. (2006). Threshold chloride concentrations of selected corrosion-resistant rebar materials compared to carbon steel. *Corrosion, 62(10),* 892–904. DOI 10.5006/1.3279899.

16. Fajardo, S., Bastidas, D. M., Criado, M., Romero, M., Bastidas, J. M. (2011). Corrosion behaviour of a new low-nickel stainless steel in saturated calcium hydroxide solution. *Construction and Building Materials, 25(11),* 4190–4196. DOI 10.1016/j.conbuildmat.2011.04.056.

17. Bautista, A., Paredes, E. C., Alvarez, S. M., Velasco, F. (2016). Welded, sandblasted, stainless steel corrugated bars in non-carbonated and carbonated mortars: a 9-year corrosion study. *Corrosion Science, 102,* 363–372. DOI 10.1016/j.corsci.2015.10.029.

18. Pérez-Quiroz, J. T., Terán, J., Herrera, M. J., Martínez, M., Genescá, J. (2008). Assessment of stainless steel reinforcement for concrete structures rehabilitation. *Journal of Constructional Steel Research, 64(11),* 1317–1324. DOI 10.1016/j.jcsr.2008.07.024.

19. Abreu, C. M., Cristóbal, M. J., Losada, R., Nóvoa, X. R., Pena, G. et al. (2004). Comparative study of passive films of different stainless steels developed on alkaline medium. *Electrochimica Acta, 49(17–18),* 3049–3056. DOI 10.1016/j.electacta.2004.01.064.

20. Abreu, C. M., Cristóbal, M. J., Losada, R., Nóvoa, X. R., Pena, G. et al. (2004). High frequency impedance spectroscopy study of passive films formed on AISI 316 stainless steel in alkaline medium. *Journal of Electroanalytical Chemistry, 572(2),* 335–345. DOI 10.1016/j.jelechem.2004.01.015.

21. Abreu, C. M., Cristóbal, M. J., Losada, R., Nóvoa, X. R., Pena, G. et al. (2006). The effect of Ni in the electrochemical properties of oxide layers grown on stainless steels. *Electrochimica Acta, 51(15),* 2991–3000. DOI 10.1016/j.electacta.2005.08.033.

22. Zheng, H., Dai, J. G., Poon, C. S., Li, W. (2018). Influence of calcium ion in concrete pore solution on the passivation of galvanized steel bars. *Cement and Concrete Research, 108,* 46–58. DOI 10.1016/j. cemconres.2018.03.001.

23. Kubissa, W., Jaskulski, R., Reiterman, P. (2017). Ecological concrete based on blast-furnace cement with incorporated coarse recycled concrete aggregate and fly ash addition. *Journal of Renewable Materials, 5(1),* 53–61. DOI 10.7569/JRM.2017.634103.

24. Feng, X., Zhang, L., Zhang, J., Lu, X., Xu, Y. et al. (2019). Effect of aluminum tri-polyphosphate on corrosion behavior of reinforcing steel in seawater prepared coral concrete. *Journal of Wuhan University of Technology-Materials Science Edition, 34(4),* 906–913. DOI 10.1007/s11595-019-2136-5.

25. Parka, J., Taea, S., Kima, T. (2012). Life cycle CO_2 assessment of concrete by compressive strength on construction site in Korea. *Renewable and Sustainable Energy Reviews, 16(5),* 2940–2946. DOI 10.1016/j. rser.2012.02.014.

26. Yoon, Y. C., Kim, K. H., Lee, S. H., Yeo, D. (2018). Sustainable design for reinforced concrete columns through embodied energy and CO_2 emission optimization. *Energy and Buildings, 174,* 44–53. DOI 10.1016/j. enbuild.2018.06.013.

27. Jing, R., Yasir, M. W., Qian, J., Zhang, Z. (2019). Assessments of greenhouse gas (GHG) emissions from stainless steel production in China using two evaluation approaches. *Environmental Progress & Sustainable Energy, 38(1),* 47–55. DOI 10.1002/ep.13125.

28. Berndt, M. L. (2015). Influence of concrete mix design on CO_2 emissions for large wind turbine foundations. *Renewable Energy, 83,* 608–614. DOI 10.1016/j.renene.2015.05.002.

29. Chau, C. K., Hui, W. K., Ng, W. Y., Powell, G. (2012). Assessment of CO_2 emissions reduction in high-rise concrete office buildings using different material use options. *Resources, Conservation and Recycling, 61,* 22–34. DOI 10.1016/j.resconrec.2012.01.001.

30. Chau, C. K., Leung, T. M., Ng, W. Y. (2015). A review on life cycle assessment, life cycle energy assessment and life cycle carbon emissions assessment on buildings. *Applied Energy, 143,* 395–413. DOI 10.1016/j. apenergy.2015.01.023.

31. JTS-153. (2015). *Standard for durability design of port and waterway engineering structures*. Beijing: CCCC Fourth Harbor Engineering Institute.

32. Yu, H., Da, B., Ma, H., Zhu, H., Yu, Q. et al. (2017). Durability of concrete structures in tropical atoll environment. *Ocean Engineering, 135,* 1–10. DOI 10.1016/j.oceaneng.2017.02.020.

33. CTL Group (2013). Service life modeling of the progreso pier. *http://www.stainlesssteelrebar.org/media/1083/ref19_case_study_of_progreso_pier.pdf*.

34. Torres-Acosta, A. A., Martínez-Madrid, M., Castro-Borges, P. (2018). Progreso's viaduct in Yucatan, Mexico: first durable concrete structure in the world made with stainless steel. *Hormigón y Acero, 69,* 35–41.

35. Mistry, M., Koffler, C., Wong, S. (2016). LCA and LCC of the world's longest pier: a case study on nickel-containing stainless steel rebar. *International Journal of Life Cycle Assessment, 21(11),* 1637–1644. DOI 10.1007/s11367-016-1080-2.

36. Alvarez, S. M., Bautista, A., Velasco, F. (2011). Corrosion behaviour of corrugated lean duplex stainless steels in simulated concrete pore solutions. *Corrosion Science, 53(5),* 1748–1755. DOI 10.1016/j.corsci.2011.01.050.

37. Chen, X., Wu, S. (2013). Influence of water-to-cement ratio and curing period on pore structure of cement mortar. *Construction and Building Materials, 38,* 804–812. DOI 10.1016/j.conbuildmat.2012.09.058.

38. Chen, D., Liao, Y., Jiang, C., Feng, X. (2013). The mechanical properties of coastal soil treated with cement. *Journal of Wuhan University of Technology-Materials Science Edition, 28(6),* 1155–1160. DOI 10.1007/s11595-013-0836-9.

39. Bertolini, L., Gastaldi, M. A. (2011). Corrosion resistance of low-nickel duplex stainless steel rebars. *Materials and Corrosion-Werkstoffe und Korrosion, 62(2),* 120–129. DOI 10.1002/maco.201005774.

40. ASTM G 59-91 (1995). *Standard test method for conducting potentiodynamic polarization resistance measurements*. Philadelphia: American Society for Testing and Materials.

41. Dong, S. G., Zhao, B., Lin, C. J., Du, R. G., Hu, R. G. et al. (2012). Corrosion behavior of epoxy/zinc duplex coated rebar embedded in concrete in ocean environment. *Construction and Building Materials, 28(1),* 72–78. DOI 10.1016/j.conbuildmat.2011.08.026.

42. Pour Ghaz, M., Isgor, O. B., Ghods, P. (2009). The effect of temperature on the corrosion of steel in concrete. Part 1: simulated polarization resistance tests and model development. *Corrosion Science, 51(2),* 415–425. DOI 10.1016/j.corsci.2008.10.034.

43. Andrade, C., Alonso, C., Gulikers, J., Polder, R., Cigna, R. et al. (2004). Test methods for on-site corrosion rate measurement of steel reinforcement in concrete by means of the polarization resistance method. *Materials and Structures, 37(9),* 623–643. DOI 10.1007/BF02483292.

44. Cao, C., Cheung, M. M. S., Chan, B. Y. B. (2013). Modelling of interaction between corrosion-induced concrete cover crack and steel corrosion rate. *Corrosion Science, 69,* 97–109. DOI 10.1016/j.corsci.2012.11.028.

45. Sánchez, M., Mahmoud, H., Alonso, M. C. (2012). Electrochemical response of natural and induced passivation of high strength duplex stainless steels in alkaline media. *Journal of Solid State Electrochemistry, 16(3),* 1193–1202. DOI 10.1007/s10008-011-1498-1.

46. García Alonso, M. C., González, J. A., Miranda, J., Escudero, M. L., Correia, M. J. et al. (2007). Corrosion behaviour of innovative stainless steels in mortar. *Cemment and Concrete Research, 37(11),* 1562–1569. DOI 10.1016/j.cemconres.2007.08.010.

47. García-Alonso, M. C., Escudero, M. L., Miranda, J. M., Vega, M. I., Capilla, F. et al. (2007). Corrosion behaviour of new stainless steels reinforcing bars embedded in concrete. *Cemment and Concrete Research, 37(10),* 1463–1471. DOI 10.1016/j.cemconres.2007.06.003.

48. Alonso, M. C., Luna, F. J., Criado, M. (2019). Corrosion behavior of duplex stainless steel reinforcement in ternary binder concrete exposed to natural chloride penetration. *Construction and Building Materials, 199,* 385–395. DOI 10.1016/j.conbuildmat.2018.12.036.

49. Otieno, M., Beushausen, H., Alexander, M. (2012). Prediction of corrosion rate in reinforced concrete structures-a critical review and preliminary results. *Materials and Corrosion-Werkstoffe und Korrosion, 63,* 777–790.

50. Broomfield, J. P., Rodriguez, J., Ortega, L. M., Garcia, A. M. (1993). Proceedings of the international symposium on condition assessment, protection, repair, and rehabilitation of concrete bridges exposed to aggressive environments, ACI fall convention, 9th-10th November. Minneapolis, MN, 644–651.

51. Gürten, A. A., Kayakırılmaz, K., Erbil, M. (2007). The effect of thiosemicarbazide on corrosion resistance of steel reinforcement in concrete. *Construction and Building Materials, 21(3),* 669–676. DOI 10.1016/j.conbuildmat.2005.12.010.

52. Deus, J. M., Díaz, B., Freire, L., Nóvoa, X. R. (2014). The electrochemical behaviour of steel rebars in concrete: an electrochemical impedance spectroscopy study of the effect of temperature. *Electrochimica Acta, 131,* 106–115. DOI 10.1016/j.electacta.2013.12.012.

53. Feng, X., Lu, X., Zuo, Y., Zhuang, N., Chen, D. (2016). Electrochemical study the corrosion behaviour of carbon steel in mortars under compressive and tensile stresses. *Corrosion Science, 103,* 66–74. DOI 10.1016/j.corsci.2015.11.006.

54. Feng, X., Zhang, X., Xu, Y., Shi, R., Lu, X. et al. (2019). Corrosion behavior of deformed low-nickel stainless steel in groundwater solution. *Engineering Failure Analysis, 98,* 49–57. DOI 10.1016/j.engfailanal.2019.01.073.

55. Liu, G., Zhang, Y., Wu, M., Huang, R. (2017). Study of depassivation of carbon steel in simulated concrete pore solution using different equivalent circuits. *Construction and Building Materials, 157,* 357–362. DOI 10.1016/j.conbuildmat.2017.09.104.

56. Pech Canul, M. A., Castro, P. (2002). Corrosion measurements of steel reinforcement in concrete exposed to a tropical marine atmosphere. *Cement and Concrete Research, 32(3),* 491–498. DOI 10.1016/S0008-8846(01)00713-X.

57. González, J. A., Molina, A., Escudero, M. L. (1985). Errors in the electrochemical evaluation of very small corrosion rates—I. polarization resistance method applied to corrosion of steel in concrete. *Corrosion Science, 25(10),* 917–930. DOI 10.1016/0010-938X(85)90021-6.

58. Poursaee, A. (2011). Corrosion measurement techniques in steel reinforced concrete. *Journal of ASTM International, 8,* 1–15.